Commun. Comput. Phys.
doi: 10.4208/cicp.181113.241014a

Vol. **xx**, No. x, pp. 1-20
xxx 201x

Fast Solution for Solving the Modified Helmholtz Equation with the Method of Fundamental Solutions

C. S. Chen[1,4], Xinrong Jiang[2], Wen Chen[1,*] and Guangming Yao[3]

[1] *Department of Engineering Mechanics, Hohai University, Nanjing, China.*
[2] *Bank of Nanjing, Nanjing, China, 210008.*
[3] *Department of Mathematics, Clarkson University, Potsdam, NY, USA.*
[4] *Department of Mathematics, University of Southern Mississippi, Hattiesburg, MS, USA.*

Received XXX; Accepted (in revised version) XXX

Communicated by Jie Shen

Abstract. The method of fundamental solutions (MFS) is known as an effective boundary meshless method. However, the formulation of the MFS results in a dense and extremely ill-conditioned matrix. In this paper we investigate the MFS for solving large-scale problems for the nonhomogeneous modified Helmholtz equation. The key idea is to exploit the exponential decay of the fundamental solution of the modified Helmholtz equation, and consider a sparse or diagonal matrix instead of the original dense matrix. Hence, the homogeneous solution can be obtained efficiently and accurately. A standard two-step solution process which consists of evaluating the particular solution and the homogeneous solution is applied. Polyharmonic spline radial basis functions are employed to evaluate the particular solution. Five numerical examples in irregular domains and a large number of boundary collocation points are presented to show the simplicity and effectiveness of our approach for solving large-scale problems.

AMS subject classifications: 65N10, 65N30

Key words: Method of fundamental solutions, method of particular solutions, boundary meshless method, polyharmonic splines, radial basis functions, modified Helmholtz equation.

1 Introduction

One of the major advantages of boundary element methods (BEMs) over finite element (FEM), finite difference (FDM) and finite volume methods (FVM) is their ability to transform the domain integral into the boundary and thus avoid domain discretization which

*Corresponding author. *Email addresses:* cschen.math@gmail.com (C. S. Chen), hawk.xrjiang@gmail.com (X. R. Jiang), chenwen@hhu.edu.cn (W. Chen), guangmingyao@gmail.com (G. Yao)

is often the most tedious and expensive part of the solution process. However, for inhomogeneous problems, domain integration is required in the formulation of BEMs which takes away their main advantage. During the past two decades, much effort in the BEM literature has been devoted to this issue with great success. The most notable schemes in this direction are the dual reciprocity method (DRM) [1] and the multiple reciprocity method (MRM) [2]. The DRM is in fact a process of evaluating the particular solution without direct numerical integration and is equivalent to the method of particular solutions (MPS). We will use the MPS due to its close connection with the method of fundamental solutions (MFS) which is the focus of this paper. Despite the advantage of mesh reduction by one dimension, the resultant matrix in the BEM formulation is dense in contrast to the sparse matrices obtained with traditional methods such as the FEM, FDM and FVM. Hence, the second major challenge for BEMs is how to overcome the necessity to solve the resulting dense systems.

Since the early 1990s, the method of fundamental solutions has re-emerged as an effective meshless method. Instead of boundary discretization as in the classical BEM, only the boundary collocation points are used in the solution process. The MFS is attributed to Kupradze in 1964 [3] and is classified as an indirect boundary method or regular BEM in the engineering literature. In the MFS, the singularity is avoided by the use of a fictitious boundary outside the domain of interest. As a result, the MFS has the following advantages over the classical BEM: (i) It requires no boundary discretization. (ii) No boundary integration is required. (iii) It converges exponentially for smooth boundary shapes and boundary data. (iv) It is attractive for solving high dimensional problems. (iv) Its implementation and coding are easy. Despite all these attractive features, the MFS was not considered as a main-stream numerical method due to its limitation in solving only homogeneous problems and the uncertainty in choosing the fictitious boundary. An important reason for which the MFS has gradually received attention from the science and engineering community is that, due to the effort of Golberg and Chen [4], it has been successfully extended to solving nonhomogeneous problems and various types of time-dependent problems by being used in conjunction the MPS. With the combined features of the MFS and the MPS, a truly meshless numerical scheme (MFS-MPS) for solving partial differential equations can be obtained. In the MFS-MPS, two dense matrix systems, one for finding the particular solution using the MPS and the other for obtaining the homogeneous solution using the MFS, need to be solved. The development of the compactly supported radial basis functions (CS-RBFs) [5] has made it possible for the matrix in the MPS to be sparse [6]. However, no progress has been reported in the effort to formulate a sparse matrix in the context of the MFS. It is desirable that MFS-MPS has the combined features of 'sparsity' and 'meshlessness'.

It is the purpose of this paper to investigate, apparently for the first time, how a sparse formulation of the MFS for the modified Helmholtz equation, which has wide applications in time-dependent PDEs [7], can be achieved.

2 The method of fundamental solutions

We first consider the following homogeneous boundary value problem

$$\left(\Delta-\lambda^2\right)v(\mathbf{x})=0, \quad \mathbf{x}\in\Omega, \tag{2.1}$$

$$v(\mathbf{x})=g_1(\mathbf{x}), \qquad \mathbf{x}\in\Gamma_1, \tag{2.2}$$

$$\frac{\partial v(\mathbf{x})}{\partial n}=g_2(\mathbf{x}), \qquad \mathbf{x}\in\Gamma_2, \tag{2.3}$$

where λ is a constant, g_1 and g_2 are known functions, Ω is a simply-connected domain, and $\Gamma_1\cup\Gamma_2=\partial\Omega$. The fundamental solution $G(\mathbf{x},\boldsymbol{\xi};\lambda)$ of (2.1) in 2D is given by

$$G(\mathbf{x},\boldsymbol{\xi};\lambda)=\frac{1}{2\pi}K_0(\lambda r), \tag{2.4}$$

where K_0 is the modified Bessel function of the second kind of order zero, and $r=\|\mathbf{x}-\boldsymbol{\xi}\|$ is the Euclidean distance between $\mathbf{x}$ and $\boldsymbol{\xi}$. We observe that both $K_0(\lambda r)$ in (2.4) are exponentially decaying function with a singularity at $r=0$. For a small argument $\lambda r, K_0(\lambda r)\approx -\ln(\lambda r)$ while for a large argument,

$$K_0(\lambda r)\approx\frac{\pi}{\sqrt{2\pi\lambda r}}\exp(-r\lambda), \qquad \text{for} \quad \lambda r\gg 1. \tag{2.5}$$

This special feature alone will lead us to a sparse matrix formulation. We shall address this issue later.

The original idea in the MFS is to approximate the solution v by v_M which can be expressed as a linear combination of fundamental solutions [3, 8]

$$v_M(\mathbf{x})=\sum_{j=1}^{M}a_k G(\mathbf{x},\boldsymbol{\xi}_j;\lambda), \quad \mathbf{x}\in\Omega, \tag{2.6}$$

where $\{\boldsymbol{\xi}_j\}_1^M$ are M distinct points on the fictitious boundary $\widehat{\Omega}$ of Ω. In general, there have been two approaches for choosing $\{\boldsymbol{\xi}_j\}_1^M$ - the fixed and the adaptive approach [4,9]. In this paper we will only focus on the fixed approach. In the fixed approach, the location of the points $\{\boldsymbol{\xi}_j\}_1^M$ is chosen a priori. Much of the work in this direction has relied on the approximation results of Bogomolny [8] and Cheng's convergence results for the Dirichlet problem for Laplace's equation when Ω and $\widehat{\Omega}$ are concentric circles [10]. In their work it was shown that the accuracy of the approximation improves as $\widehat{\Omega}$ moves away from Ω. Cheng's result was generalized by Katsurada and Okamoto [11–14] who showed that if Ω is a closed Jordan curve in the plane and the data is analytic, then

$$\|v-v_M\|_\infty\leq c(r_1/r_2)^M,$$

where r_1 and r_2 are the diameters of Ω and $\widehat{\Omega}$ respectively. As a consequence, we can deduce that choosing the source points $\{\boldsymbol{\xi}_j\}_1^M$ to be equally spaced around a circle of

radius r_2 in $\mathbb{R}^2$ and equally spaced in polar co-ordinates (ϕ,θ) on a sphere of radius r_2 in $\mathbb{R}^3$, provides excellent results. We refer the reader for the detailed implementation to Reference [15].

Once the source points have been chosen, the coefficients $\{a_j\}_1^M$ in (2.6) are usually obtained by collocation. That is, M points $\{\mathbf{x}_k\}_1^M$ are chosen on $\partial\Omega$ and then the coefficients $\{a_j\}_1^M$ satisfy the equations

$$\sum_{j=1}^{M} a_j G(\mathbf{x}_k,\boldsymbol{\xi}_j;\lambda)=g_1(\mathbf{x}_k), \qquad 1\le k\le l, \tag{2.7}$$

$$\sum_{j=1}^{M} a_j \frac{\partial}{\partial n} G(\mathbf{x}_k,\boldsymbol{\xi}_j;\lambda)=g_2(\mathbf{x}_k), \quad l+1\le k\le M, \tag{2.8}$$

where $\{\mathbf{x}_k\}_1^l\in\Gamma_1$ and $\{\mathbf{x}_k\}_{l+1}^M\in\Gamma_2$. Let us denote by $\mathbf{a}=[a_1\ a_2\cdots a_M]^T$, $\mathbf{g}=[g_1(\mathbf{x}_1)\ g_1(\mathbf{x}_2)\ \cdots\ g_1(\mathbf{x}_l)\ \ g_2(\mathbf{x}_{l+1})\cdots\ g_2(\mathbf{x}_M)]^T$ and

$$\mathbf{G}_{11}=\begin{bmatrix} G_{11} & \cdots & G_{1M} \\ \vdots & \cdots & \vdots \\ G_{l1} & \cdots & G_{lM} \end{bmatrix}, \quad \mathbf{G}_{21}=\begin{bmatrix} \widetilde{G}_{(l+1)1} & \cdots & \widetilde{G}_{(l+1)M} \\ \vdots & \cdots & \vdots \\ \widetilde{G}_{M1} & \cdots & \widetilde{G}_{MM} \end{bmatrix}, \tag{2.9}$$

where $G_{kj}=G(\mathbf{x}_k,\boldsymbol{\xi}_j;\lambda)$, $\widetilde{G}_{kj}=\frac{\partial}{\partial n}G(\mathbf{x}_k,\boldsymbol{\xi}_j;\lambda)$. Then Eqs. (2.7)-(2.8) can be rewritten into the matrix form

$$\mathbf{A}\mathbf{a}=\mathbf{g}, \tag{2.10}$$

where

$$\mathbf{A}=\begin{bmatrix} \mathbf{G}_{11} \\ \mathbf{G}_{21} \end{bmatrix}. \tag{2.11}$$

Because the MFS matrix $\mathbf{A}$ becomes highly ill-conditioned as r_2 increases, we usually limit the length of r_2 to about $5\sim10$ times the diameter of Ω. Despite the ill-conditioning, the accuracy of the numerical solution is largely unaffected [4, 9].

For large M, the MFS system for the dense matrix $\mathbf{A}$ is also expensive to solve, especially in the 3D case. As may be observed, the coefficients of $\mathbf{A}$ are largely dependent on the type of boundary conditions, λ, and r which depend on the geometrical shape of the domain. Due to the exponential decay of $G(\mathbf{x},\boldsymbol{\xi};\lambda)$ in (2.4) and (2.5), the coefficients of $\mathbf{A}$ in (2.11) are very small and the discrepancy between the maximum and minimum values in the elements of $\mathbf{A}$ becomes large, as we shall see, for large λ. Hence, a large number of the elements of G_{kj} and $\widetilde{G}_{kj}$ in $\mathbf{A}$ are so small that they can be neglected. As a result, the linear system of equations (2.10) becomes a sparse system. Such an approach has been widely used in data compression in image processing. In our case, we can consider the coefficient matrix of $\mathbf{A}$ as a digital image.

Based on the observation that the fundamental solution of the modified Helmholtz equation decays exponentially with respect to r and λ, we can make use of this property

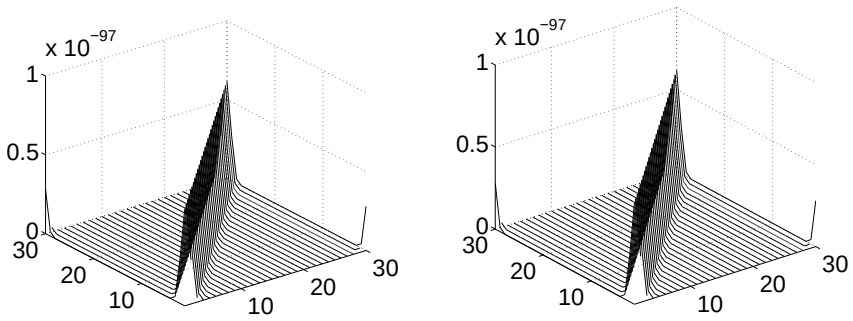

Figure 1: The profile of **A** before (left) and after (right) the truncation.

to reduce the dense matrix **A** in (2.11) to a sparse matrix and thus pave the way for solving large-scale problems using the MFS. To illustrate the simple idea mentioned above, we consider the modified Helmholtz equation (2.1) with a Dirichlet boundary condition (2.2) only. Let $\lambda^2 = 1000$ and Ω be the unit circle and the fictitious boundary be a concentric circle with radius 8. We choose 30 collocation points evenly distributed on the physical boundary and the same number of points on the fictitious boundary. It is note worthy that the structure of **A** is independent of the boundary condition $g_1(\mathbf{x})$ in (2.2). The maximum and minimum coefficients of **A** are $\varepsilon_1 = 6.167 \times 10^{-98}$ and $\varepsilon_2 = 1.855 \times 10^{-125}$ respectively. Even though they are all very small in magnitude, there is a wide margin between ε_1 and ε_2. Let the truncation level be $\varepsilon = 10^{-100}$. This means we set coefficient $G_{kj} = 0$ if $|G_{kj}| < \varepsilon$. In this case, there are 150 nonzero entries in **A** which implies the ratio of nonzero elements with respect to the full matrix is 1/6. The profiles of the matrix **A** before and after truncation are shown in Fig. 1. As we can see the images of these two figures are indistinguishable after 85% of the coefficients of **A** are set to zero. The distribution of nonzero elements of **A** is shown in Fig. 2. As we shall see in a later section, the numerical accuracy will remain unchanged after the matrix **A** becomes sparse.

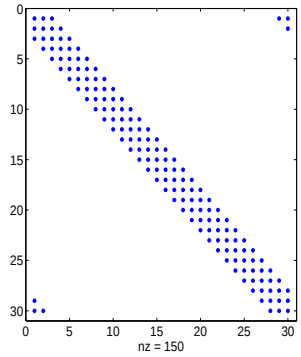

Figure 2: The profile of the nonzero entries for the MFS matrix after the truncation in Fig. 1 (right).

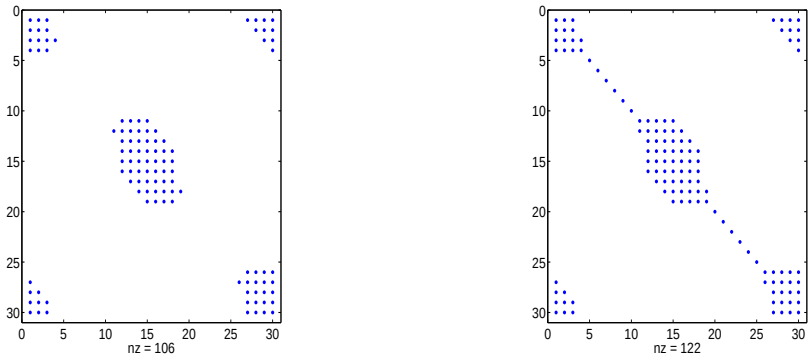

Figure 3: The profile of nonzero entries of the MFS matrix without (left) and with (right) keeping diagonal entries.

Instead of a circle, we consider the above problem for the domain $\Omega=\{(x,y):x^2/9+y^2\leq 1\}$. The number of collocation points and the location of the fictitious points are chosen to be the same as before. We found that the maximum and minimum coefficients of $\mathbf{A}$ are $\varepsilon_1=2.139\times 10^{-70}$ and $\varepsilon_2=5.723\times 10^{-153}$ respectively. The difference of the exponents between ε_1 and ε_2 in this case is larger than in the previous one. If we choose $\varepsilon=10^{-85}$, the density of nonzero entries in $\mathbf{A}$ is 14%. Note that the matrix becomes singular after the truncation as shown in Fig. 3 (left). As one can see, the dominant nonzero entries are located along most of the diagonal and four corners of the matrix. To ensure the non-singularity of $\mathbf{A}$, we avoid to truncate the elements on the diagonal even though their values are less than ε. The modified version of the profile of $\mathbf{A}$ after the truncation is shown in Fig. 3 (right). As we shall see later, such a step is necessary to ensure the solvability of the truncated system.

3 The method of particular solutions

In this section, we extend the MFS to solving inhomogeneous equations by introducing the method of particular solutions [4]. We consider the following inhomogeneous boundary value problem

$$\left(\Delta-\lambda^2\right)u(\mathbf{x})=f(\mathbf{x}),\quad \mathbf{x}\in\Omega, \tag{3.1}$$

$$u(\mathbf{x})=g_1(\mathbf{x}),\quad \mathbf{x}\in\Gamma_1, \tag{3.2}$$

$$\frac{\partial u(\mathbf{x})}{\partial n}=g_2(\mathbf{x}),\quad \mathbf{x}\in\Gamma_2. \tag{3.3}$$

A particular solution u_p satisfies

$$\left(\Delta-\lambda^2\right)u_p(\mathbf{x})=f(\mathbf{x}) \tag{3.4}$$

but does not necessarily satisfy the boundary conditions (3.2)-(3.3). Let $v=u-u_p$. Then v satisfies

$$\left(\Delta-\lambda^2\right)v(\mathbf{x})=0, \qquad \mathbf{x}\in\Omega, \tag{3.5}$$

$$v(\mathbf{x})=g_1(\mathbf{x})-u_p(\mathbf{x}), \qquad \mathbf{x}\in\Gamma_1, \tag{3.6}$$

$$\frac{\partial v(\mathbf{x})}{\partial n}=g_2(\mathbf{x})-\frac{\partial u_p(\mathbf{x})}{\partial n}, \quad \mathbf{x}\in\Gamma_2. \tag{3.7}$$

Note that in this process the inhomogeneous equations were split into two parts: the particular solution u_p and the homogeneous solution v. The homogeneous equations (3.5)-(3.7) can be solved by the MFS as discussed in the previous section. It is well-known that u_p in (3.4) is not unique, and there are various techniques for the numerical approximation of u_p. An efficient way of obtaining it is using the method of particular solutions (MPS) through radial basis functions (RBFs) [4].

To approximate the particular solutions u_p in (3.4) using RBFs, f is first approximated by a polyharmonic spline $\widehat{f}$; i.e.,

$$\widehat{f}(\mathbf{x})=\sum_{j=1}^{N}\alpha_j\varphi_j^{[n]}(\mathbf{x})+p_n, \tag{3.8}$$

where

$$\begin{aligned} p_n&=\sum_{i=1}^{\ell_n}\beta_i b_i(\mathbf{x}),\\ \varphi_j^{[n]}(\mathbf{x})&=\begin{cases} r_j^{2n}\log r_j, & n\geq 1 \ \text{ in } \mathbb{R}^2,\\ r_j^{2n-1}, & n\geq 1 \ \text{ in } \mathbb{R}^3, \end{cases} \end{aligned} \tag{3.9}$$

$\{b_i\}_1^{\ell_n}$ is a basis for polynomials of degree $\leq n$,$r_j=\|\mathbf{x}-\mathbf{x}_j\|$ and $\{\mathbf{x}_j\}_1^N\subseteq\Omega$ is a unisolvent set of points for polynomial interpolation. In addition, if the coefficient $\{\alpha_j\}_1^N$ satisfy

$$\sum_{j=1}^{N}\alpha_j b_i(\mathbf{x}_j)=0, \quad 1\leq i\leq \ell_n, \tag{3.10}$$

then, for a given $\widehat{f}$, there is a unique polyharmonic spline interpolant to f of the form (3.8) on $\{\mathbf{x}_j\}_1^N$. To be more specific, if the condition

$$f(\mathbf{x}_k)=\widehat{f}(\mathbf{x}_k), \quad 1\leq k\leq N,$$

is imposed, then the linear system

$$\begin{cases} \widehat{f}(\mathbf{x}_k)=\displaystyle\sum_{j=1}^{N}\alpha_j\varphi_j^{[n]}(\mathbf{x}_k)+\sum_{i=1}^{\ell_n}\beta_i b_i(\mathbf{x}_k), & 1\leq k\leq N,\\ \displaystyle\sum_{j=1}^{N}\alpha_j b_i(\mathbf{x}_j)=0, & 1\leq i\leq \ell_n, \end{cases} \tag{3.11}$$

is uniquely solvable.

Hence, to obtain approximate particular solutions to (3.4), we approximate f by $\widehat{f}$ and solve (3.11). Then, from (3.4),

$$\left(\Delta-\lambda^2\right)u_p(\mathbf{x})=f(\mathbf{x})\simeq\sum_{j=1}^{N}\alpha_j\varphi_j^{[n]}(\mathbf{x}_k)+\sum_{i=1}^{\ell_n}\beta_i b_i(\mathbf{x}_k). \tag{3.12}$$

By linearity,

$$u_p(\mathbf{x})\simeq\hat{u}_p(\mathbf{x})=\sum_{j=1}^{N}\alpha_j\Phi_j^{[n]}(\mathbf{x}_k)+\sum_{i=1}^{\ell_n}\beta_i\chi_i(\mathbf{x}_k), \tag{3.13}$$

where

$$\left(\Delta-\lambda^2\right)\Phi=\varphi_j^{[n]}, \tag{3.14}$$

$$\left(\Delta-\lambda^2\right)\chi_i^{[n]}=b_i. \tag{3.15}$$

In $\mathbb{R}^2$ the explicit forms of $\Phi^{[n]}$,$1\le n\le 4$, are given in Table 1 [16], where $\gamma\simeq 0.5772156649015328$ is Euler's constant, $K_0(\cdot)$ is the modified Bessel function of the third kind with order zero. The $\chi_i^{[n]}$ can be obtained using the formulas derived in [17]. It can be shown that a solution of

$$\Delta W-\lambda^2 W=x^m y^n$$

is given by

$$W(x,y)=\sum_{k=0}^{\left[\frac{m}{2}\right]}\sum_{\ell=0}^{\left[\frac{n}{2}\right]}\frac{(-1)^{k+\ell+1}(k+\ell)!m!n!x^{m-2k}y^{n-2\ell}}{\lambda^{2k+2\ell+2}k!\ell!(m-2k)!(n-2\ell)!} \tag{3.16}$$

with a similar formula in $\mathbb{R}^3$ [18]. Note that W can be obtained easily by using symbolic computation packages such as MATHEMATICA or MAPLE.

We note that no particular solution using globally defined radial basis functions other than polyharmonic splines has been derived for the modified Helmholtz differential operator. Furthermore, the resultant matrix of the system of equations in (3.11) is also dense which is not desirable in term of computational efficiency as we have indicated earlier in Section 2.

The approximate homogeneous solution v_M in (3.5)-(3.7) can be obtained by solving (2.7)-(2.8) with $g_1(\mathbf{x}_k)$ and $g_2(\mathbf{x}_k)$ replaced by $g_1(\mathbf{x}_k)-\widehat{u}_p(\mathbf{x}_k)$ and $g_2(\mathbf{x}_k)-\partial\widehat{u}_p(\mathbf{x}_k)/\partial n$, respectively.

One system instead of two can be obtained as follows. The approximate solution $\widehat{u}$ of (3.1)-(3.3) can be written as

$$\widehat{u}(\mathbf{x})=v_M+\widehat{u}_p=\sum_{j=1}^{M}a_j G(\mathbf{x},\boldsymbol{\xi}_j;\lambda)+\sum_{j=1}^{N}\alpha_j\psi_j^{[n]}+\sum_{i=1}^{\ell_n}\beta_i\chi_i^{[n]}. \tag{3.17}$$

Table 1: Polyharmonic splines and the corresponding particular solutions.

$\varphi^{[n]}$	$\psi^{[n]}$
$r^2\log r$	$\begin{cases} -\frac{4}{\lambda^4}(K_0(\lambda r)+\log r)-\frac{r^2\log r}{\lambda^2}-\frac{4}{\lambda^4}, & r>0 \\ \frac{4}{\lambda^4}\left(\gamma+\log\left(\frac{\lambda}{2}\right)\right)-\frac{4}{\lambda^4}, & r=0 \end{cases}$
$r^4\log r$	$\begin{cases} -\frac{64}{\lambda^6}(K_0(\lambda r)+\log r)-\frac{r^2\log r}{\lambda^2}\left(\frac{16}{\lambda^2}+r^2\right)-\frac{8r^2}{\lambda^4}-\frac{96}{\lambda^6}, & r>0 \\ \frac{64}{\lambda^6}\left(\gamma+\log\left(\frac{\lambda}{2}\right)\right)-\frac{96}{\lambda^6}, & r=0 \end{cases}$
$r^6\log r$	$\begin{cases} -\frac{2304}{\lambda^8}(K_0(\lambda r)+\log r)-\frac{r^2\log r}{\lambda^2}\left(\frac{576}{\lambda^4}+\frac{36r^2}{\lambda^2}+r^4\right) \\ -\frac{12r^2}{\lambda^4}\left(\frac{40}{\lambda^2}+r^2\right)-\frac{4224}{\lambda^8}, & r>0 \\ \frac{2304}{\lambda^8}\left(\gamma+\log\left(\frac{\lambda}{2}\right)\right)-\frac{4224}{\lambda^8}, & r=0 \end{cases}$
$r^8\log r$	$\begin{cases} -\frac{147456}{\lambda^{10}}(K_0(\lambda r)+\log r)-\frac{r^2}{\lambda^4}\left(\frac{39936}{\lambda^4}+\frac{1344r^2}{\lambda^2}+16r^4\right) \\ -\frac{r^2\log r}{\lambda^2}\left(\frac{36864}{\lambda^6}+\frac{2304r^2}{\lambda^4}+\frac{64r^4}{\lambda^2}+r^6\right)-\frac{307200}{\lambda^{10}}, & r>0 \\ \frac{147456}{\lambda^{10}}\left(\gamma+\log\left(\frac{\lambda}{2}\right)\right)-\frac{307200}{\lambda^{10}}, & r=0 \end{cases}$

Substituting (3.17) into (3.1)-(3.3), we obtain the following system

$$\begin{bmatrix} \mathbf{0} & \boldsymbol{\varphi}^{[n]} \\ \mathbf{G}_{11} & \boldsymbol{\psi}^{[n]} \\ \mathbf{G}_{21} & \dfrac{\partial \boldsymbol{\psi}^{[n]}}{\partial n} \end{bmatrix} \begin{bmatrix} \mathbf{a} \\ \boldsymbol{\alpha} \end{bmatrix} = \begin{bmatrix} \mathbf{f} \\ \mathbf{g} \end{bmatrix}, \tag{3.18}$$

where

$$\boldsymbol{\varphi}^{[n]} = \begin{bmatrix} \varphi_1^{[n]}(\mathbf{x}_1) & \cdots & \varphi_1^{[n]}(\mathbf{x}_N) & b_1(\mathbf{x}_1) & \cdots & b_1(\mathbf{x}_{\ell_n}) \\ \vdots & \cdots & \vdots & \vdots & \cdots & \vdots \\ \varphi_N^{[n]}(\mathbf{x}_1) & \cdots & \varphi_N^{[n]}(\mathbf{x}_N) & b_{\ell_n}(\mathbf{x}_1) & \cdots & b_{\ell_n}(\mathbf{x}_{\ell_n}) \end{bmatrix},$$

$$\boldsymbol{\psi}^{[n]} = \begin{bmatrix} \psi_1^{[n]}(\mathbf{x}_1) & \cdots & \psi_1^{[n]}(\mathbf{x}_N) & \chi_1(\mathbf{x}_1) & \cdots & \chi_1(\mathbf{x}_{\ell_n}) \\ \vdots & \cdots & \vdots & \vdots & \cdots & \vdots \\ \psi_N^{[n]}(\mathbf{x}_1) & \cdots & \psi_N^{[n]}(\mathbf{x}_N) & \chi_{\ell_n}(\mathbf{x}_1) & \cdots & \chi_{\ell_n}(\mathbf{x}_{\ell_n}) \end{bmatrix},$$

$$\frac{\partial \boldsymbol{\psi}^{[n]}}{\partial n}=\begin{bmatrix} \frac{\partial \psi_1^{[n]}(\mathbf{x}_1)}{\partial n} & \cdots & \frac{\partial \psi_1^{[n]}(\mathbf{x}_N)}{\partial n} & \frac{\partial \chi_1(\mathbf{x}_1)}{\partial n} & \cdots & \frac{\partial \chi_1(\mathbf{x}_{\ell_n})}{\partial n} \\ \vdots & \cdots & \vdots & \vdots & \cdots & \vdots \\ \frac{\partial \psi_N^{[n]}(\mathbf{x}_1)}{\partial n} & \cdots & \frac{\partial \psi_N^{[n]}(\mathbf{x}_N)}{\partial n} & \frac{\partial \chi_{\ell_n}(\mathbf{x}_1)}{\partial n} & \cdots & \frac{\partial \chi_{\ell_n}(\mathbf{x}_{\ell_n})}{\partial n} \end{bmatrix},$$

$$\boldsymbol{\alpha}=[\alpha_1\cdots\alpha_N\ \beta_1\cdots\beta_{\ell_n}]^T,\quad \mathbf{f}=[f(\mathbf{x}_1)\cdots f(\mathbf{x}_1)]^T,\quad \mathbf{g}=[g(\mathbf{x}_1)\cdots g(\mathbf{x}_1)]^T,$$

and $\mathbf{0}$ is the zero matrix of order $N\times M$. If CS-RBFs are used as basis functions, then the block matrix $\boldsymbol{\varphi}^{[n]}$ in (3.18) is sparse. This part alone has the largest dimension in the whole matrix system. With other sparse block matrices $\mathbf{G}_{11}$ and $\mathbf{G}_{21}$, the whole matrix system in (3.18) is largely sparse. For nonlinear and time-dependent problems, such a formulation is more convenient while the formulation with two smaller matrix systems discussed earlier is slightly more efficient.

4 Numerical results

To validate the effectiveness of the proposed method for the nonhomogeneous modified Helmholtz equation, five examples have been presented. The computations were carried out using MATLAB on an AMD Athlon^{64} PC in OS Window 7.

To measure the accuracy, we place n random test points within the computational domain. The error will be evaluated according to the following definition:

$$Error=\sqrt{\frac{\sum_{i=1}^{n}(u_i-\bar{u}_i)^2}{\sum_{i=1}^{n}u_i^2}},$$

where u_i and $\bar{u}_i$ are the exact and approximate solutions at the test points x_i, respectively.

Example 4.1. To investigate how the accuracy is affected after reducing the dense matrix to a sparse matrix as shown in Section 2, we consider the following nonhomogeneous modified Helmholtz boundary value problem

$$\begin{aligned} &\left(\Delta-\lambda^2\right)u(x,y)=(1-\lambda^2)(e^x+e^y), && (x,y)\in\Omega,\\ &u(x,y)=e^x+e^y, && (x,y)\in\partial\Omega, \end{aligned}$$

where Ω is a star-shaped domain bounded by the following parametric equation (see Fig. 4)

$$\partial\Omega=\{(x,y)\,|\,x=\rho\cos\theta,\ y=\rho\sin\theta,\ 0\le\theta\le 2\pi\},$$

where

$$\rho=1+\cos^2(4\theta).$$

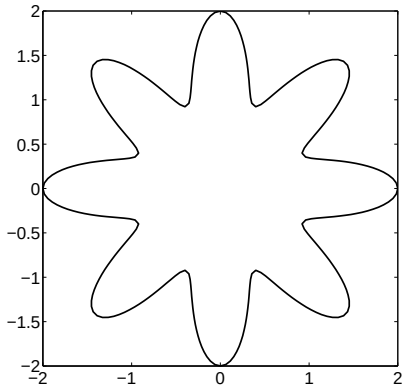

Figure 4: The star-shape domain.

To test the accuracy, we choose 100 randomly distributed points inside the domain. The points $\{(x_i,y_i)\}_1^{400}$ are the boundary collocation points. The source points $\{(s_i,t_i)\}_1^{400}$ are located very close to the boundary; with $s_i=1.001x_i$, $t_i=1.001y_i$. For the evaluation of the particular solution, we choose 441 uniformly distributed interpolation points on $[-2,2]\times[-2,2]$. For the radial basis functions, we choose polyharmonic splines of order 4 ($r^8\log r$).

For $\lambda^2=1000$, the maximum and minimum entries of the full MFS matrix are 3.57095 and 1.12517×10^{-56} respectively. In Table 2, it is interesting to note that the accuracy remains unchanged no matter how we truncate the nonzero entries of **A** in (2.11). In the bottom line of the table, the 0.25% means that **A** is essentially a diagonal matrix. In other words, for each boundary collocation point we need only the nearest source point for the evaluation of the coefficients $\{a_j\}_1^M$ in (2.7) and (2.8). This implies that we do not even need to solve the sparse system of linear equations. As a result, the computational algorithm is extremely efficient. Furthermore, we do not have to store the large matrix system. This allows us to solve problems using a very large number of boundary collocation points. As for smaller λ value, we also obtain satisfactory results. For $\lambda^2=16,25,36$, the errors are $8.27E-4, 1.99E-4$, and $6.34E-5$, respectively.

In the implementation of the MFS, the selection of the source points is often an important issue. We denote by $s_i=r*x_i, t_i=r*y_i$ as shown in the last two paragraphs. In Table 3, we present the results of using various source locations and the same number of interpolation, test points, and boundary collocation points as showed in Table 2. We observe that the closer the source points are to the boundary collocation points, the better the accuracy.

In the next four examples we will only use the diagonal elements of **A** to solve the large-scale problems. The source points will be selected as close to the boundary collocation points as possible. We believe that the errors are mostly caused by the approximation of the particular solution using polyharmonic splines.

Table 2: Sparseness of the MFS matrix versus error for $\lambda^2=1000$.

% of nonzero entry	Error
100	$2.44E-6$
92	$2.45E-6$
44	$2.45E-6$
4.8	$2.45E-6$
0.25	$2.45E-6$

Table 3: Error verses various λ^2.

r	Error ($\lambda^2=25$)	Error ($\lambda^2=100$)
1.0001	$1.06E-4$	$1.90E-6$
1.001	$1.98E-4$	$2.79E-6$
1.01	$4.24E-4$	$6.86E-6$
1.1	$1.06E-3$	$2.25E-5$
2.1	$3.08E-3$	$8.22E-4$

Example 4.2. In this example, we consider the following nonhomogeneous modified Helmholtz boundary value problem

$$\begin{aligned}&\left(\Delta-\lambda^2\right)u(x,y)=(1-\lambda^2)(\sinh x+\cosh y), && (x,y)\in\Omega,\\ &u(x,y)=\sinh x+\cosh y, && (x,y)\in\partial\Omega,\end{aligned}$$

where λ is a constant and Ω is a simply-connected domain bounded by the following parametric equation which is known as the Cassini curve (see Fig. 5)

$$\partial\Omega=\{(x,y)\,|\,x=\rho\cos\theta,\ y=\rho\sin\theta,\ 0\le\theta\le 2\pi\},$$

where

$$\rho=\left(\cos(3\theta)+\sqrt{2-\sin^2(3\theta)}\right)^{1/3}.$$

The analytical solution is given by

$$u(x,y)=\sinh x+\cosh y.$$

To test the accuracy of the method, we choose 1000 randomly distributed interior points as test points. To evaluate the particular solution, we choose 2500 uniformly distributed grid points on a square covering the domain as the interpolation points and polyharmonic splines of order 1,2,3, and 4 as the radial basis function basis. For evaluating the homogeneous solution using the MFS, we choose the source points to be congruent to the boundary collocation points with a ratio of $r=1.05$. The λ is chosen to be 30. In Fig. 6, we show the number of boundary collocation points N versus the error for various orders of polyharmonic splines. As we can see in the this figure, the overall accuracy

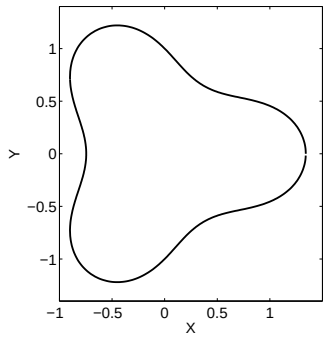

Figure 5: The computational domain.

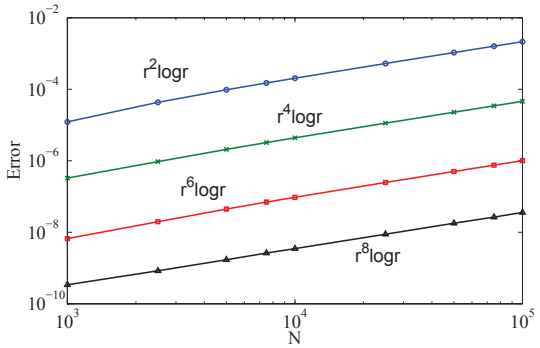

Figure 6: The number of boundary collocation points N versus the error using various order of polyharmonic splines.

is greatly affected by the order of the polyharmonic splines being used. This is consistent with the results reported in the literature [16]. We have noticed that the numerical accuracy deteriorates with the increase of the number of boundary collocation points.

Since the polyharmonic splines of order 4 is superior to the other three lower order cases, we will only be using $r^8 \log r$ in the sequel.

To show how λ affects the numerical accuracy, we choose the same number of interpolation points, source points, and 4th order of polyharmonic splines as mentioned above and 10,000 boundary collocation points. As we can see in Fig. 7, the highest accuracy is obtained for the highest λ. This is expected since the fundamental solution $K_0(\lambda r)$ decays more rapidly for higher λ. Hence, the influence of the nearby source points is more pronounced than the far away source points.

In Fig. 8, we show the efficiency of the proposed method. We use the same interpolation points, test points, source points, λ as used in the last two figures. The most time consuming part of the numerical procedure is the evaluation of the particular solutions. The evaluation of the homogeneous solution is considerably less expensive. As we can see in this figure, the computer time needed for 100,000 boundary points is only 483 seconds.

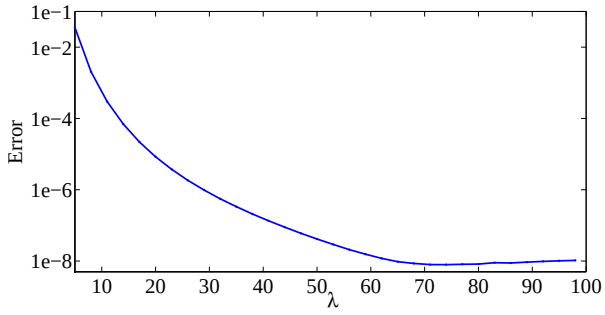

Figure 7: The higher the λ, the better the accuracy.

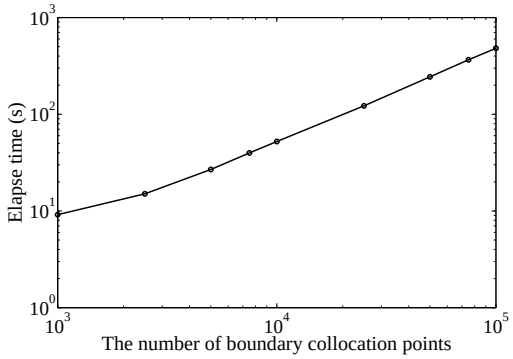

Figure 8: Elapsed computer time for various number of collocation points.

Example 4.3. In this example, we consider a more challenging near-singular problem as follows:

$$\begin{aligned}&(\Delta-2500)u(x,y)=f(x,y), && (x,y)\in\Omega,\\ &u(x,y)=g(x,y), && (x,y)\in\partial\Omega,\end{aligned}$$

where domain Ω is the same as the one in the last example, a is a constant, and

$$g(x,y)=\frac{x^2+y^2}{a-\sqrt{x^2+y^2}},\quad f(x,y)=\frac{4a^2-3a\sqrt{x^2+y^2}+(x^2+y^2)}{(a-\sqrt{x^2+y^2})^3}-2500g(x,y). \tag{4.1}$$

The analytical solution is given by

$$u(x,y)=\frac{x^2+y^2}{a-\sqrt{x^2+y^2}},\quad (x,y)\in\Omega\cup\partial\Omega.$$

For illustration, the profile of $f(x,y)$ for $a=1.9$ in (4.1) is shown in Fig. 9 where three sharp spikes occur on the boundary. Due to these sharp spikes, the numerical solution of the problem becomes very challenging.

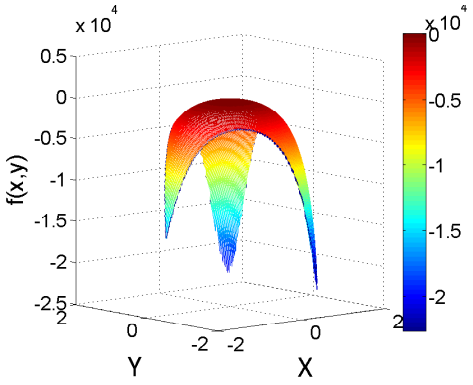

Figure 9: The profile of $f(x,y)$ for $a=1.9$.

To evaluate the particular solution, we choose 625 uniformly distributed points on a square covering the domain and the polyharmonic splines of order 4 as the radial basis function. For the MFS, we choose 500 boundary collocation points. The source points are chosen to be congruent to the boundary points with a ratio of $r=1.01$.

From Table 4, we observe that the largest sharp spike $\max(f)$ is very visible for smaller a and the errors are poor. For larger a, the forcing term becomes smoother and the accuracy improves.

Table 4: Errors for various a.

a	$\max(f)$	Error
2.80	-673.2	$1.12E-06$
2.20	-835.6	$2.80E-06$
2.00	-1101.2	$2.94E-05$
1.90	-1196.2	$1.39E-04$
1.80	-1309.2	$1.51E-03$

Example 4.4. We consider the following nonhomogeneous modified Helmholtz boundary value problem

$$\begin{aligned}&(\Delta-900)\,u(x,y)=-899(e^x+e^y), && (x,y)\in\Omega,\\ &u(x,y)=e^x+e^y, && (x,y)\in\partial\Omega,\end{aligned}$$

where Ω is a multi-connected domain bounded between an amoeba-like curve ($\partial\Omega_1$) and a small circle with center at (0,0) and radius 0.08 ($\partial\Omega_2$) (see Fig. 10). The parametric equation of the amoeba curve is as follows:

$$\partial\Omega_1=\{(x,y)\,|\,x=\rho\cos\theta,\ y=\rho\sin\theta,\ 0\le\theta\le 2\pi\},$$

where

$$\rho=e^{\sin\theta}\sin^2(2\theta)+e^{\cos\theta}\cos^2(2\theta).$$

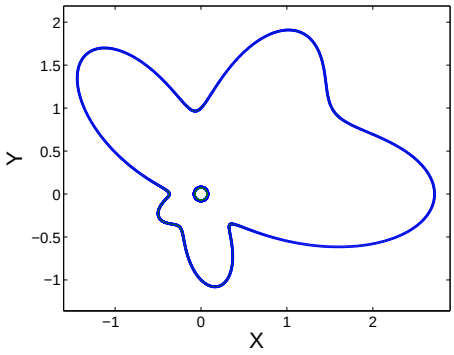

Figure 10: The computational domain.

The analytical solution is given by

$$u(x,y) = e^x + e^y.$$

To evaluate the particular solution, we employed 900 uniform grid points on a square covering the interior of the amoeba. 1000 randomly distributed points are chosen as the test points. To evaluate the homogeneous solution, we choose 10,000 points on each of the boundaries $\partial\Omega_1$ and $\partial\Omega_2$. We choose the source points outside $\partial\Omega_1$ by multiplying the boundary collocation points on $\partial\Omega_1$ by 1.0001. Similarly, we choose the source points inside $\partial\Omega_2$ by multiplying the boundary collocation points on $\partial\Omega_2$ by 0.88.

Fig. 11 shows the numerical accuracy profile using various orders of polyharmonic splines. Similar to the last example, higher accuracy can be achieved by using a higher

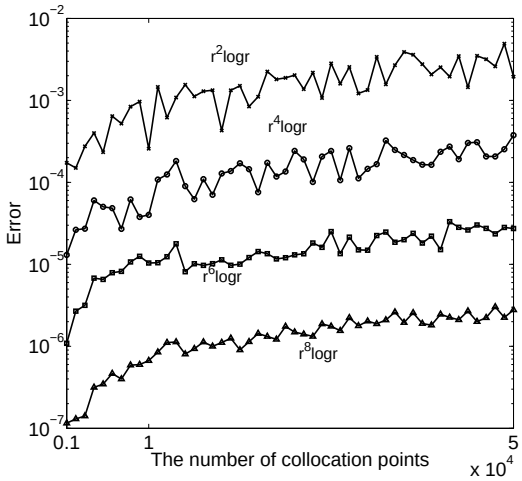

Figure 11: The accuracy profile using various orders of polyharmonic splines and numbers of boundary collocation points.

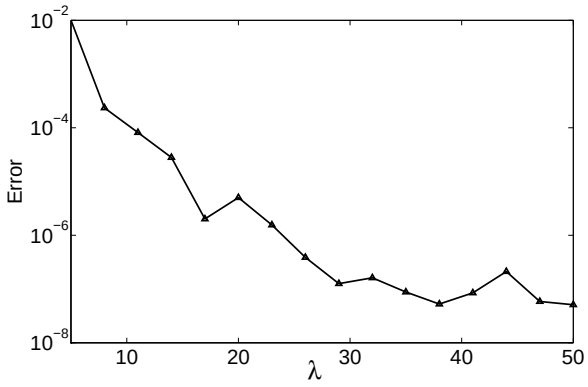

Figure 12: The numerical accuracy for λ.

order of polyharmonic splines. As a result, we will use only polyharmonic splines of order four ($r^8 \log r$) in the remaining numerical tests.

If we replace $\lambda^2 = 900$ by other numbers, we obtain a similar profile of accuracy as showed in the last example (see Fig. 12).

Despite a large amount of densely clouded boundary points as showed in the previous and current examples, we can still obtain excellent numerical results.

Example 4.5. In this example, we consider the same equation as in Example 2 but with a more complicated multi-connected domain which consists of a square domain with side length 2 and many smaller square holes lying inside (see Fig. 13). The width of each hole is 0.08. On the exterior boundary of the square, we place 1500 collocation points. Meanwhile, on the boundary of each interior square hole, we place 100 collocation points. We place the source points as close to the boundary as possible. The exterior source

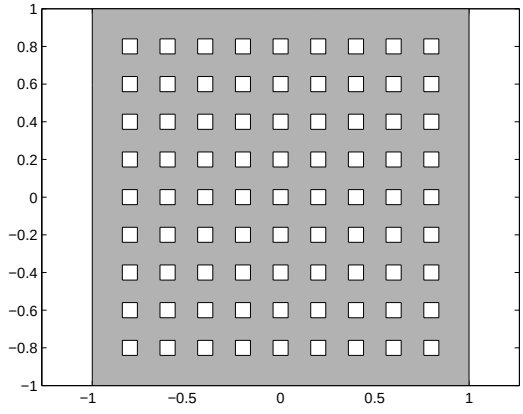

Figure 13: The computational domain.

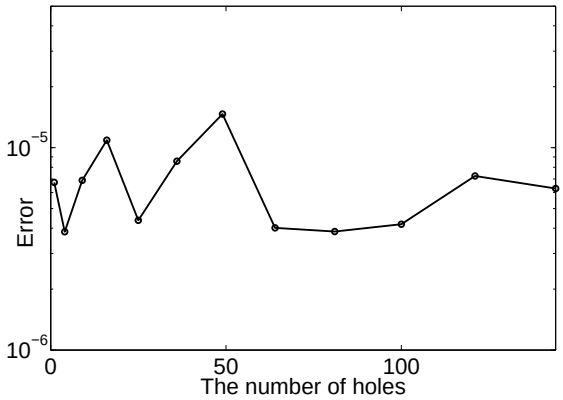

Figure 14: The error profile of using various numbers of interior square holes.

points are selected by multiplying the exterior boundary points by 1.002. Similarly, the interior source points are selected by multiplying the interior boundary points by 0.98. For the evaluation of the particular solution, we choose 900 evenly distributed points on a square covering the entire domain. We also choose 1000 randomly distributed test points for testing the error. As shown in Fig. 13, we consider up to 144 interior holes inside the square. As one can see in Fig. 14, despite the increase in boundary collocation points when more square holes are added, the accuracy remains excellent.

5 Conclusions

When the MFS is applied to solve problems in simple geometries, only a small number of boundary collocation points is usually required. The MFS is very effective due to its exponential convergence rate. In this paper we extend the MFS for solving nonhomogeneous modified Helmholtz problems in the context of fast computation and large-scale problems. The proposed method is limited to the nonhomogeneous modified Helmholtz equation. However, many differential equations can be reformulated to yield the modified Helmholtz equation. For example, time-dependent problems such as the diffusion and wave equations can be reduced to solving a series of modified Helmholtz equations using various time difference schemes. Using the Laplace transform, these types of equations can also be converted to the modified Helmholtz equation. Hence, the proposed method has the potential to efficiently solve a large class of partial differential equations. The application of the proposed approach to time-dependent problems is currently under investigation.

Our proposed approach actually resembles a localized method instead of a global method. In practice, we only use the nearest source point instead of all the source points to obtain the homogeneous solution. The proposed numerical procedure is not only meshless but also matrixless for obtaining the homogeneous solution.

In the literature, a closed-form particular solution for the modified Helmholtz equation using compactly supported radial basis functions is still not available. This hinders our effort to implement the localized approach for evaluating a particular solution of the modified Helmholtz equation. The recent developments in the localized method of particular solutions [19] can potentially provide a local scheme to evaluate these particular solutions. In this way, our proposed approach will be completely localized. The suggestion of a referee to use the idea of non-harmonic boundary condition for solving Laplace equation by Li et al. [15] could provide a way to handle the homogeneous problem. These two issues and the application to time-dependent problems will be the topics of future research.

Acknowledgments

The authors wish to thank the referees for their comments and suggestions. The research of the third author is financially supported by the National Science Funds for Distinguished Young Scholars of China (Grant No. 11125208), the National Science Funds of China (Grant Nos. 11372097, 11302069), and the 111 Project (Grant No. B12032).

References

[1] P. Partridge, C. Brebbia, and L. Wrobel, The Dual Reciprocity Boundary Element Method, CMP/Elsevier, 1992.
[2] A. Nowak and A. Neves, The multiple reciprocity boundary element method, Computational Mechanics Publications, 1994.
[3] V. Kupradze and M. Aleksidze, The method of functional equations for the approximate solution of certain boundary value problems, U.S.S.R. Computational Mathematics and Mathematical Physics, 4 (1964), 82–126.
[4] M. Golberg and C. Chen, The method of fundamental solutions for potential, Helmholtz and diffusion problems, in: M. Golberg (Ed.), Boundary Integral Methods: Numerical and Mathematical Aspects, WIT Press, (1998), 103–176.
[5] H. Wendland, Piecewise polynomial, positive definite and compactly supported radial functions of minimal degree, Adv. Comput. Math., 4 (1995), 389–396.
[6] C. Chen, C. Brebbia and H. Power, Dual reciprocity method using compactly supported radial basis functions, Comm. Num. Meth. Eng., 15 (1999), 137–150.
[7] H. Cho, M. Golberg, A. Muleshkov and X. Li, Trefftz methods for time dependent partial differential equations, Computers, Materials, and Continua, 1 (2004), 1–38.
[8] A. Bogomolny, Fundamental solutions method for elliptic boundary value problems, SIAM J. Numer. Anal., 22 (1985), 644–669.
[9] G. Fairweather and A. Karageorghis, The method of fundamental solution for elliptic boundary value problems, Advances in Computational Mathematics, 9 (1998), 69–95.
[10] R. Cheng, Delta-trigonometric and Spline Methods using the Single-layer Potential Representation, Ph.D. thesis, University of Maryland (1987).
[11] M. Katsurada and H. Okamoto, A mathematical study of the charge simulation method, Journal of the Faculty of Science, University of Tokyo, Section 1A, 35 (1988), 507–518.

[12] M. Katsurada, Asymptotic error analysis of the charge simulation method in a Jordan region with an analytic boundary, Journal of the Faculty of Science of Tokyo University, Section 1A, 37 (1990), 635–657.
[13] M. Katsurada, Charge simulation method using exterior mapping functions, Japan Journal of Industrial and Applied Mathematics, 11 (1994), 47–61.
[14] M. Katsurada and H. Okamoto, The collocation points of the fundamental solution method for the potential problem, Computers and Mathematics with Applications, 31 (1996), 123–137.
[15] M. Li, C.S. Chen and A. Karageorghis, The MFS for the solution of harmonic boundary value problems with non-harmonic boundary conditions, Computers and Mathematics with Applications, 66 (2013), 2400–2424.
[16] A. Muleshkov, M. Golberg and C.S. Chen, Particular solutions of Helmholtz-type operators using higher order polyharmonic splines, Comp. Mech. 23 (1999) 411–419.
[17] A. Muleshkov, C.S Chen, M. Golberg and A.-D. Cheng, Analytic particular solutions for inhomogeneous Helmholtz-type equations, in: S. Atluri, F. Brust (Eds.), Advances in Computational Engineering & Sciences, Tech Science Press, (2000) 27–32.
[18] M. Golberg, A. Muleshkov, C.S. Chen and A.-D. Cheng, Polynomial particular solutions for certain kind of partial differential operators, Numerical Methods for Partial Differential Equations, 19 (2003), 112–133.
[19] G. Yao, C.S. Chen, J. Kolibal, A localized approach for the method of approximate particular solutions, Computers and Mathematics with Applications, 61 (2011), 545–559.